

Supplemental Material for

Integration of negative, zero and positive linear thermal expansion makes borate optical crystals light transmission temperature-independent

Xingxing Jiang^{a,b+}, Naizheng Wang^{a,h+}, Liyuan Dong^c, Maxim S. Molokeev^{d,i,j}, Shuaihua Wang^e, Youquan Liu^{a,b}, Shibin Guo^f, Wei Li^g, Rongjin Huang^f, Shaofan Wu^e, Laifeng Li^f, Zheshuai Lin^{a,b,h*}

^a *Functional Crystals Lab, Technical Institute of Physics and Chemistry, Chinese Academy of Sciences, Beijing 100190, China.*

^b *Center of Materials Science and Optoelectronics Engineering, University of Chinese Academy of Sciences, Beijing 100049, China*

^c *School of Science, Jiangsu University of Science and Technology, Zhenjiang 212100, China*

^d *Laboratory of Crystal Physics, Kirensky Institute of Physics, Federal Research Center KSC SB RAS, Krasnoyarsk 660036, Russia*

^e *Fujian Institute of Research on the Structure of Matter, Chinese Academy of Sciences, Fuzhou, Fujian 350002, China.*

^f *Key Laboratory of Cryogenics, Technical Institute of Physics and Chemistry, Chinese Academy of Sciences, Beijing 100190, China*

^g *School of Materials Science and Engineering; TKL of Metal and Molecule-Based Material Chemistry, Nankai University, Tianjin 300350, China*

^h *University of the Chinese Academy of Sciences, Beijing 100049, China*

ⁱ *Department of Physics, Far Eastern State Transport University, Khabarovsk 680021, Russia*

^j *Siberian Federal University, Krasnoyarsk 660041, Russia*

⁺Contribute equally

Email: zslin@mail.ipc.ac.cn

Experimental and calculation details

Powder samples synthesis. Polycrystalline AEB_2O_4 was synthesized by a solid-state reaction in a stoichiometric ratio with $Sr/CaCO_3$ and B_2O_3 as the starting materials, and to compensate for the loss resulting from volatilization, B_2O_3 was excessive by ten percent. The ingredients were mixed homogeneously, heated gradually to $800^{\circ}C$, and kept at that temperature in air for 3 days with careful intermediate grinding. After cooling to room temperature, white powders of Sr/CaB_2O_4 were obtained.

Crystal growth. The crystals of AEB_2O_4 were grown by top-seed method. High purity (Aldrich 99.9%) CaO and B_2O_3 were chosen as the raw materials, and stoichiometric amounts of CaO and B_2O_3 powder were well mixed in a ball mill at 300 r/min for 10 h. The mixture was sintered in an air atmosphere at $1000^{\circ}C$ for 24 h, cooled to room temperature, and then transferred into a Ø80 mm platinum crucible in a molten salt furnace. The temperature of the furnace was increased to $1200^{\circ}C$ with a heating rate of $10^{\circ}C/min$ and was held for 24 h to homogenize the melt. Afterwards, an Ø3 mm platinum wire was placed on the melt surface, and crystallization of CaB_2O_4 could be obtained by spontaneous nucleation as the temperature decreased ($\sim 1105^{\circ}C$). The spontaneously crystallized crystal was adopted as the seed for regrowth following the above process, and a single crystal in centimeter-sized can be obtained. The crystal growth method of SrB_2O_4 was similar to the above procedure of CaB_2O_4 .

Variable-temperature powder X-ray diffraction. Variable temperature X-ray diffraction patterns were recorded from 13 K to 1080 K with an internal voltage of 20 K. Each pattern was written down with Bruker D8 advanced X-ray diffractometer Cu $K\alpha$ radiation ($K\alpha 1=1.5406\text{\AA}$ and $K\alpha 2=1.5443\text{\AA}$) on the finely grounded powder samples. The angular scanning range was set to 10° to 90° with a step of 0.01° and scanning rate of 0.05 s/step. The cell parameters under different temperatures were refined by the Lebail method using the TOPAS 4.2 program¹. The thermal expansion coefficients based on the refined cell parameters were fitted by PASCal software².

Variable-temperature Raman spectrum. By equipped with a solid-state laser with a wavelength of 532 nm, LabRAM HR Evolution was applied to collect the Raman spectrum of AEB_2O_4 . The spectra were recorded from 100 to 1700 cm^{-1} at temperatures in the range of 93 K-500 K with an interval of 20 K.

Optical transmittance. The deep ultraviolet transmission spectra were recorded by a VUVas2000 McPherson spectrophotometer in the wavelength range of 150–200 nm. UV-Vis transmission spectra were collected with a Varian Cary 5000 scan UV-Vis-NIR spectrophotometer over the spectral range of 200-1500 nm at room temperature. The infrared spectrum was obtained at room temperature in a range from 400 to 4000 cm^{-1} with a resolution of 1 cm^{-1} via an Excalibur HE 3100 spectrometer. The infrared absorption edges at the respective temperatures were predicted by a two-phonon absorption approximation using the highest frequency in the variable-temperature Raman spectra³.

Theoretical Calculations. First-principle calculations were performed by CASTEP software⁴ based on plane-wave pseudopotential density functional theory (DFT)^{4, 5}. The exchange-correlation energy was described by the functionals developed by Perdew, Burke, and Ernzerhof (PBE)⁶ within the framework of the generalized

gradient approximation (GGA)⁷. The effective interaction between the valence electrons and atom cores was modeled by optimized norm-conserving pseudopotential⁸ in the Kleiman-Bylander form⁹, which allows the usage of a relatively small plane-wave basis set without compromising the computational accuracy. A kinetic energy cutoff of 900 eV and Monkhorst-Pack¹⁰ k-point mesh spanning less than 0.04 Å⁻¹ in the Brillouin zone were chosen. The theoretical atomic coordination at various temperatures was refined by geometry optimization with the cell parameters fixed on their experimental values, in which the Broyden–Fletcher–Goldfarb–Shanno (BFGS)¹¹ minimization scheme was used. The theoretical Raman spectra and phonon spectrum were calculated via linear response method developed by Baroni *et al*¹², in which the force constants matrix characterizing the effective atomic interaction were calculated by differentiating the Hellmann-Feynman forces on atoms, with respect to ionic coordinates. By the linear response calculation, the frequency, intensity, and exact atomic vibration of the phonon modes can be obtained. Then, by comparing the experimental and calculated Raman spectra, the corresponding theoretical counterparts and the exact atomic vibration of the respective modes in experimental Raman spectra are determined. The electronic band structure of AEB_2O_4 was calculated by hybridized PBE0 functionals¹³, which have been proven to be able to accurately predict the band gaps of borates¹⁴. Based on the electronic band structures at respective temperatures, the imaginary part of the dielectric function was calculated based on the electronic transition between valence bands and conduction bands, and accordingly, the real part of the dielectric function, *i.e.*, refractive index (n), was determined using the Kramers–Kronig transform¹⁵. Thermo-optical coefficients were fitted based on the calculated refractive index at various temperatures.

Method to achieve the direction with temperature-independent optical path.

Because the space group of AEB_2O_4 ($Pbcn$) belongs to the orthorhombic system, their crystallographic axes are consistent with the optical principal axes and thermodynamic axes. In this case, one needs to simply find a direction (θ, φ) to make

$$K_{\text{thermal expansion}}(\theta, \varphi) = K_{\text{thermal - optical}}(\theta, \varphi) \quad (\text{S1})$$

where $K_{\text{thermal expansion}}(\theta, \varphi)$ and $K_{\text{thermal - optical}}(\theta, \varphi)$ are the values of thermal expansion and thermal optical coefficients, respectively, along the (θ, φ) direction.

In the equation (R4), $K_{\text{thermal expansion}}(\theta, \varphi)$ and $K_{\text{thermal - optical}}(\theta, \varphi)$ can be obtained by the angle transformation:

$$K_{\text{thermal expansion}}(\theta, \varphi) = A^T K_{\text{thermal expansion}}^{xyz} A \quad (\text{S2})$$

$$K_{\text{thermal - optical}}(\theta, \varphi) = A^T K_{\text{thermal - optical}}^{xyz} A \quad (\text{S3})$$

where $K_{\text{thermal expansion}}^{xyz}$ and $K_{\text{thermal - optical}}^{xyz}$ are the matrices of thermal expansion and thermal optical coefficients, respectively, in the principal axis coordinate system (x, y and z), and A is the direction vector with respect to the coordinate axes:

$$A = \begin{pmatrix} \cos(\varphi)\sin(\theta) \\ \sin(\varphi)\sin(\theta) \\ \cos(\theta) \end{pmatrix} \quad (\text{S4})$$

By the above operations, the direction with temperature-independent optical path can be obtained.

Fig. S1 Variable-temperature XRD patterns of (a) CaB_2O_4 and (b) SrB_2O_4 from 13K to 1080K.

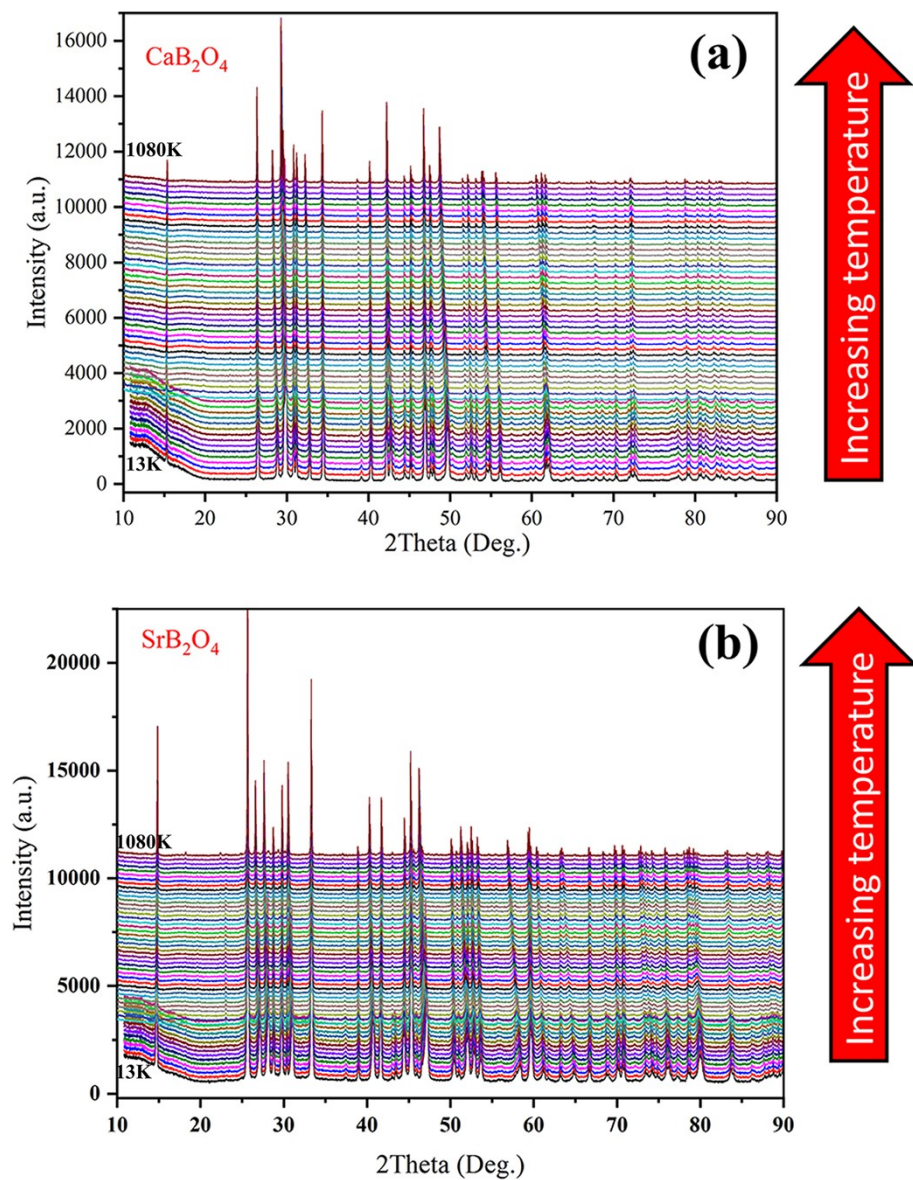


Fig. S2 Refinement plots for the XRD patterns at (a) 13K; (b) 280K; (c) 1080K in CaB_2O_4 , and (d) 13K; (e) 280K; (f) 1080K in SrB_2O_4 .

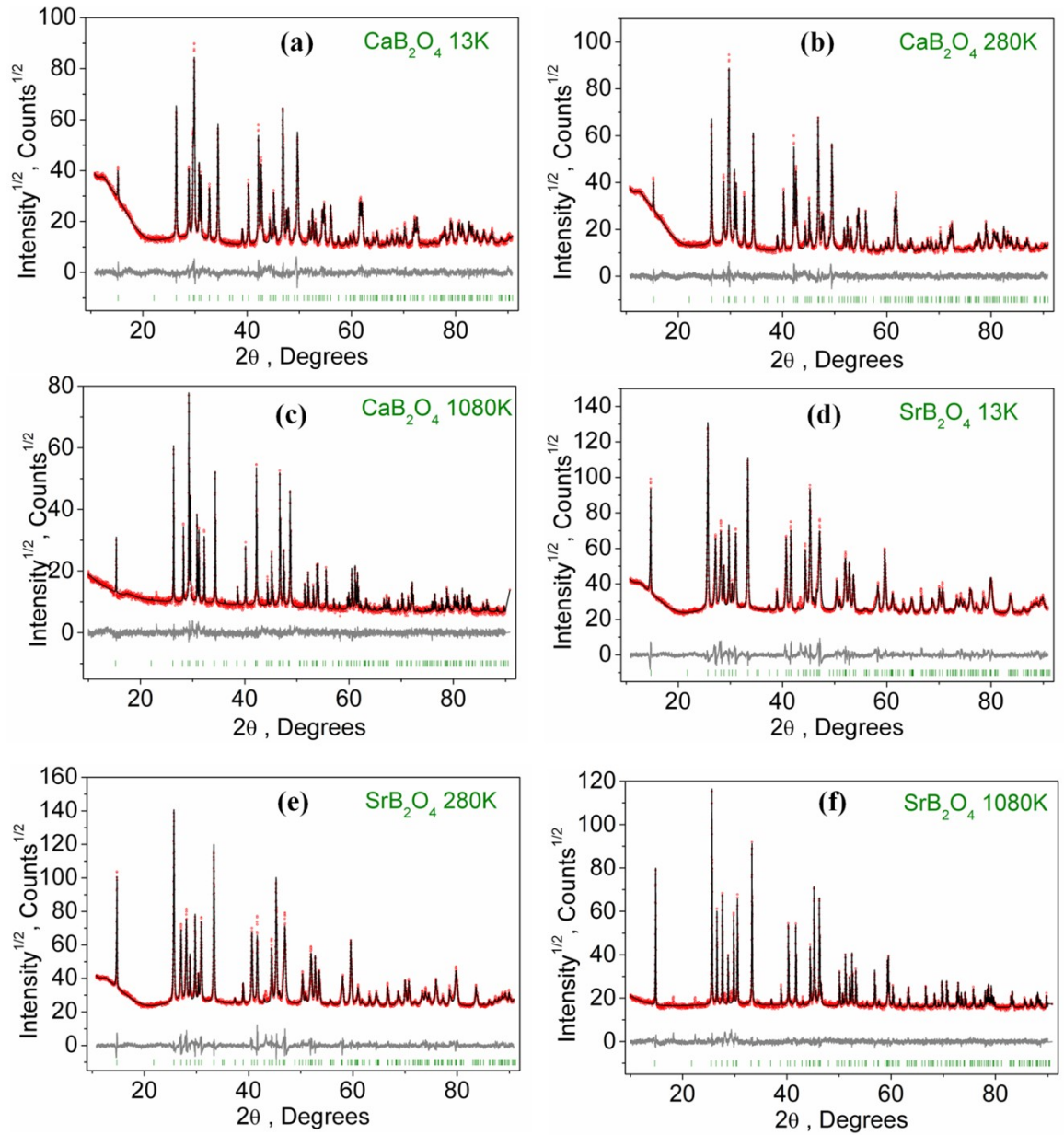


Table S1 Refined cell parameters of AEB_2O_4 from 13K to 1080K

Temperature (K)	CaB ₂ O ₄			SrB ₂ O ₄		
	<i>a</i> (Å)	<i>b</i> (Å)	<i>c</i> (Å)	<i>a</i> (Å)	<i>b</i> (Å)	<i>c</i> (Å)
13	11.5999 (4)	4.2804 (1)	6.1853 (2)	12.0034 (4)	4.3370 (1)	6.5589 (2)
20	11.6000 (3)	4.2804 (9)	6.1853 (1)	12.0036 (4)	4.3371 (1)	6.5589 (2)
40	11.5995 (3)	4.2803 (9)	6.1858 (1)	12.0040 (3)	4.3371 (1)	6.5609 (2)
60	11.5992 (6)	4.2801 (2)	6.1870 (3)	12.0032 (3)	4.3363 (1)	6.5653 (2)
80	11.5991 (3)	4.2800 (1)	6.1885 (2)	12.0031 (3)	4.3363 (9)	6.5668 (2)
100	11.5988 (3)	4.2799 (1)	6.1899 (2)	12.0029 (5)	4.3360 (2)	6.5684 (3)
120	11.5990 (3)	4.2799 (1)	6.1917 (2)	12.0027 (3)	4.3359 (1)	6.5698 (2)
140	11.5986 (3)	4.2797 (1)	6.1933 (2)	12.0022 (3)	4.3355 (1)	6.5714 (2)
160	11.5992 (5)	4.2799 (2)	6.1958 (3)	12.0019 (4)	4.3353 (1)	6.5733 (2)
180	11.6001 (3)	4.2800 (1)	6.1987 (2)	12.0018 (4)	4.3349 (1)	6.5755 (2)
200	11.6001 (6)	4.2799 (2)	6.2012 (3)	12.0020 (4)	4.3349 (1)	6.5780 (2)
220	11.5998 (3)	4.2798 (1)	6.2038 (2)	12.0029 (5)	4.3349 (2)	6.5812 (3)
240	11.6003 (2)	4.2798 (8)	6.2066 (1)	12.0033 (3)	4.3347 (1)	6.5839 (2)
260	11.6002 (2)	4.2796 (9)	6.2091 (1)	12.0037 (4)	4.3346 (1)	6.5865 (2)
280	11.6006 (5)	4.2795 (2)	6.2120 (3)	12.0040 (3)	4.3344 (9)	6.5900 (2)
300	11.6013 (4)	4.2798 (1)	6.2152 (2)	12.0042 (3)	4.3345 (1)	6.5923 (2)
320	11.6019 (5)	4.2797 (2)	6.2194 (3)	12.0038 (3)	4.3345 (1)	6.5990 (2)
340	11.6036 (6)	4.2800 (2)	6.2232 (3)	12.0053 (3)	4.3347 (1)	6.6037 (2)
360	11.6038 (5)	4.2799 (2)	6.2269 (3)	12.0062 (5)	4.3347 (2)	6.6074 (3)
380	11.6053 (4)	4.2803 (2)	6.2305 (2)	12.0064 (3)	4.3346 (1)	6.6109 (2)
400	11.6058 (4)	4.2804 (2)	6.2337 (2)	12.0078 (3)	4.3349 (1)	6.6145 (2)
420	11.6075 (5)	4.2808 (2)	6.2373 (3)	12.0081 (3)	4.3348 (1)	6.6182 (2)
440	11.6086 (4)	4.2810 (2)	6.2408 (2)	12.0091 (4)	4.3350 (1)	6.6216 (2)
460	11.6097 (5)	4.2814 (2)	6.2440 (3)	12.0103 (7)	4.3352 (3)	6.6255 (4)
480	11.6108 (5)	4.2815 (2)	6.2475 (2)	12.0112 (3)	4.3352 (9)	6.6286 (2)
500	11.6118 (4)	4.2818 (2)	6.2505 (2)	12.0115 (2)	4.3352 (8)	6.6322 (2)
520	11.6123 (4)	4.2818 (2)	6.2537 (2)	12.0126 (3)	4.3355 (1)	6.6358 (2)
540	11.6141 (3)	4.2824 (1)	6.2571 (2)	12.0130 (6)	4.3355 (2)	6.6390 (3)
560	11.6141 (4)	4.2822 (2)	6.2598 (3)	12.0144 (3)	4.3355 (1)	6.6422 (2)
580	11.6162 (3)	4.2828 (1)	6.2635 (2)	12.0157 (3)	4.3360 (8)	6.6464 (2)
600	11.6170 (4)	4.2831 (1)	6.2666 (2)	12.0165 (3)	4.3360 (9)	6.6497 (2)
620	11.6183 (4)	4.2834 (2)	6.2699 (2)	12.0179 (4)	4.3364 (1)	6.6531 (2)
640	11.6195 (4)	4.2837 (1)	6.2731 (2)	12.0178 (4)	4.3362 (2)	6.6563 (3)
660	11.6205 (4)	4.2839 (1)	6.2764 (2)	12.0199 (2)	4.3367 (9)	6.6603 (2)
680	11.6216 (4)	4.2843 (1)	6.2796 (2)	12.0208 (2)	4.3369 (7)	6.6642 (1)
700	11.6230 (3)	4.2846 (1)	6.2831 (2)	12.0216 (2)	4.3370 (7)	6.6671 (1)
720	11.6244 (3)	4.2850 (1)	6.2864 (2)	12.0234 (2)	4.3375 (7)	6.6713 (1)
740	11.6250 (3)	4.2851 (1)	6.2897 (2)	12.0236 (2)	4.3375 (6)	6.6753 (1)
760	11.6263 (3)	4.2854 (1)	6.2930 (2)	12.0253 (2)	4.3378 (6)	6.6778 (1)
780	11.6279 (2)	4.2859 (8)	6.2968 (1)	12.0259 (3)	4.3380 (1)	6.6813 (2)

800	11.6291 (3)	4.2862 (1)	6.3003 (2)	12.0281 (2)	4.3385 (5)	6.6854 (9)
820	11.6304 (3)	4.2865 (1)	6.3038 (2)	12.0288 (2)	4.3386 (5)	6.6891 (1)
840	11.6318 (3)	4.2869 (1)	6.3075 (2)	12.0300 (1)	4.3389 (5)	6.6926 (9)
860	11.6324 (3)	4.2871 (1)	6.3107 (2)	12.0306 (1)	4.3390 (5)	6.6962 (9)
880	11.6344 (3)	4.2877 (1)	6.3145 (2)	12.0322 (1)	4.3394 (5)	6.7002 (8)
900	11.6347 (2)	4.2877 (7)	6.3178 (1)	12.0329 (1)	4.3396 (5)	6.7044 (8)
920	11.6369 (1)	4.2884 (5)	6.3220 (7)	12.0342 (1)	4.3399 (5)	6.7081 (8)
940	11.6381 (2)	4.2887 (6)	6.3255 (9)	12.0362 (1)	4.3404 (4)	6.7121 (7)
960	11.6392 (2)	4.2890 (5)	6.3293 (8)	12.0368 (1)	4.3406 (4)	6.7157 (7)
980	11.6410 (2)	4.2897 (9)	6.3334 (1)	12.0383 (1)	4.3408 (4)	6.7194 (6)
1000	11.6420 (2)	4.2898 (9)	6.3369 (1)	12.0399 (1)	4.3413 (4)	6.7234 (6)
1020	11.6431 (2)	4.2901 (8)	6.3408 (1)	12.0410 (1)	4.3415 (3)	6.7270 (6)
1040	11.6448 (2)	4.2906 (8)	6.3450 (1)	12.0421 (1)	4.3418 (4)	6.7308 (6)
1060	11.6473 (2)	4.2913 (7)	6.3496 (1)	12.0437 (1)	4.3422 (3)	6.7350 (6)
1080	11.6487 (1)	4.2918 (5)	6.3542 (5)	12.0449 (1)	4.3425 (4)	6.7391 (6)

Fig. S3 Refined cell parameter versus temperature in (a) CaB_2O_4 and (b) SrB_2O_4 from 13K to 1080K. The temperature range (13 to 280K) for coexisting NTE, ZTE and PTE is highlighted by blue color, and that (above 280K) for normal PTE along all the three axes is highlighted by yellow color respectively.

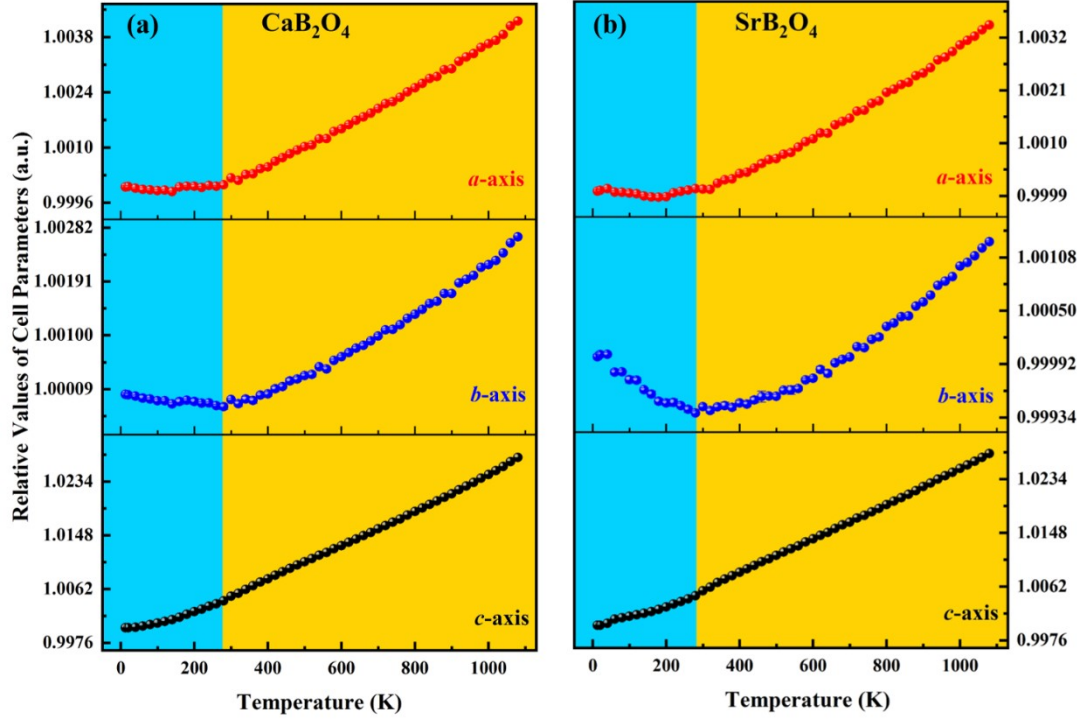


Table S2 Linear thermal expansion coefficient(α_l), thermo-optical coefficient(α_n) along thermal and optical principal X , Y , and Z -axes, minimum optical path fluctuation and optimal direction for the minimum optical path fluctuation in AEB_2O_4 , quartz, sapphire, diamond and CaF_2 . The minimum optical path fluctuation is defined as the minimum value of the sum between thermo-optic coefficient and thermal expansion coefficient. All the optical path values at the integer angles closest to the matching curve in AEB_2O_4 are listed in TABLE S3.

Materials	$\alpha_n(X)$ (/ MK)	$\alpha_n(Y)$ (/ MK)	$\alpha_n(Z)$ (/ MK)	$\alpha_l(X)$ (/ MK)	$\alpha_l(Y)$ (/ MK)	$\alpha_l(Z)$ (/ MK)	The minimum optical path fluctuation (/ MK)	Optimal transmission direction for the minimum optical path fluctuation ($^{\circ}, ^{\circ}$)	Reference
CaB_2O_4	-2.98	-3.84	-4.75	0.29	-0.62	16.50	less than ~0.1	listed in TABLE S3	This work
SrB_2O_4	-3.64	-4.49	-5.77	0.09	-2.39	16.95	less than ~0.1	listed in TABLE S3	This work
SiO_2	-3.18	-3.18	-2.51	20.80	20.80	12.30	9.12	(90, 0)	¹⁶
Al_2O_3	7.33	7.33	6.65	7.70	7.70	7.00	13.65	(θ , 0)	¹⁷
Diamond	4.04	4.04	4.04	0.70	0.70	0.70	4.74	(θ , φ)	^{18, 19}
CaF_2	-7.32	-7.32	-7.32	18.85	18.85	18.85	11.53	(θ , φ)	^{20, 21}

Table S3 Sum of linear thermal expansion coefficient and thermo-optical coefficient (γ) at the integer angles closest to the matching curve in AEB_2O_4 . Because the matching curve is continuous in space, for each integer polar angle φ there has a corresponding integer azimuth angle θ closest to the curve. Since the matching curve is symmetrical with respect to (X, Y) , (X, Z) and (Y, Z) planes, only the values in the first quadrant (*i.e.*, $0 \leq \theta \leq 90^\circ$, and $0 \leq \varphi \leq 90^\circ$) are displayed, and those in the other quadrants can be easily obtained by symmetry operation.

CaB ₂ O ₄				SrB ₂ O ₄			
(θ, φ) (°, °)	γ (/MK)	(θ, φ) (°, °)	γ (/MK)	(θ, φ) (°, °)	γ (/MK)	(θ, φ) (°, °)	γ (/MK)
(64,0)	-0.0496	(61,45)	0.0145	(60,0)	-0.0954	(55,45)	-0.1327
(64,1)	-0.0492	(61,46)	0.0383	(60,1)	-0.0946	(55,46)	-0.0935
(64,2)	-0.0479	(61,47)	0.0620	(60,2)	-0.0923	(55,47)	-0.0543
(64,3)	-0.0457	(61,48)	0.0857	(60,3)	-0.0885	(55,48)	-0.0152
(64,4)	-0.0426	(61,49)	0.1092	(60,4)	-0.0831	(55,49)	0.0237
(64,5)	-0.0387	(60,50)	-0.0988	(60,5)	-0.0762	(55,50)	0.0625
(64,6)	-0.0339	(60,51)	-0.0759	(60,6)	-0.0678	(55,51)	0.1010
(64,7)	-0.0282	(60,52)	-0.0532	(60,7)	-0.0579	(54,52)	-0.1384
(64,8)	-0.0217	(60,53)	-0.0307	(60,8)	-0.0466	(54,53)	-0.1015
(64,9)	-0.0143	(60,54)	-0.0085	(60,9)	-0.0337	(54,54)	-0.0649
(64,10)	-0.0061	(60,55)	0.0135	(60,10)	-0.0193	(54,55)	-0.0288
(64,11)	0.0029	(60,56)	0.0352	(60,11)	-0.0036	(54,56)	0.0069
(64,12)	0.0127	(60,57)	0.0566	(60,12)	0.0137	(54,57)	0.0420
(64,13)	0.0234	(60,58)	0.0777	(60,13)	0.0321	(54,58)	0.0766
(64,14)	0.0348	(60,59)	0.0984	(60,14)	0.0521	(54,59)	0.1107
(64,15)	0.0470	(60,60)	0.1188	(60,15)	0.0734	(53,60)	-0.1440
(64,16)	0.0500	(59,61)	-0.1024	(60,16)	0.0961	(53,61)	-0.1121
(64,17)	0.0737	(59,62)	-0.0833	(59,17)	-0.1091	(53,62)	-0.0809
(64,18)	0.0881	(59,63)	-0.0647	(59,18)	-0.0844	(53,63)	-0.0505
(63,19)	-0.1002	(59,64)	-0.0465	(59,19)	-0.0585	(53,64)	-0.0208
(63,20)	-0.0847	(59,65)	-0.0289	(59,20)	-0.0314	(53,65)	0.0080
(63,21)	-0.0685	(59,66)	-0.0117	(59,21)	-0.0031	(53,66)	0.0360
(63,22)	-0.0516	(59,67)	0.0049	(59,22)	0.0263	(53,67)	0.0631
(63,23)	-0.0342	(59,68)	0.0209	(59,23)	0.0567	(53,68)	0.0894
(63,24)	-0.0161	(59,69)	0.0364	(59,24)	0.0882	(53,69)	0.11468
(63,25)	0.0026	(59,70)	0.0513	(58,25)	-0.1176	(53,70)	0.13898
(63,26)	0.0218	(59,71)	0.0655	(58,26)	-0.0849	(52,71)	-0.1368
(63,27)	0.0415	(59,72)	0.0791	(58,27)	-0.0512	(52,72)	-0.1152
(63,28)	0.0618	(59,73)	0.0921	(58,28)	-0.0167	(52,73)	-0.0945
(63,29)	0.0825	(59,74)	0.1044	(58,29)	0.0186	(52,74)	-0.0750

(62,30)	0.1037	(59,75)	0.1160	(58,30)	0.0546	(52,75)	-0.0565
(62,31)	-0.0876	(58,76)	-0.1235	(58,31)	0.0916	(52,76)	-0.0391
(62,32)	-0.0660	(58,77)	-0.1135	(57,32)	-0.1188	(52,77)	-0.0228
(62,33)	-0.0440	(58,78)	-0.1042	(57,33)	-0.0814	(52,78)	-0.0078
(62,34)	-0.0216	(58,79)	-0.0957	(57,34)	-0.0435	(52,79)	0.0062
(62,35)	0.0010	(58,80)	-0.0878	(57,35)	-0.0050	(52,80)	0.0190
(62,36)	0.0240	(58,81)	-0.0807	(57,36)	0.0339	(52,81)	0.0305
(62,37)	0.0471	(58,82)	-0.0743	(57,37)	0.0733	(52,82)	0.0409
(62,38)	0.0706	(58,83)	-0.0688	(57,38)	0.1131	(52,83)	0.0500
(62,39)	0.0942	(58,84)	-0.0639	(56,39)	-0.1049	(52,84)	0.0579
(61,40)	-0.1039	(58,85)	-0.0598	(56,40)	-0.0654	(52,85)	0.0645
(61,41)	-0.0803	(58,86)	-0.0565	(56,41)	-0.0256	(52,86)	0.0699
(61,42)	-0.0568	(58,87)	-0.0540	(56,42)	0.01429	(52,87)	0.0740
(61,43)	-0.0330	(58,88)	-0.0522	(56,43)	0.05435	(52,88)	0.0769
(61,44)	-0.0092	(58,89)	-0.0512	(56,44)	0.0945	(52,89)	0.0785

Table S4 Theoretically refined bond lengths and angles at variable temperature in AEB_2O_4 .

Temperature (K)	CaB ₂ O ₄				SrB ₂ O ₄			
	Average length of B-O bonds (Å)	Average length of Ca-O bonds (Å)	Angle of $\angle B-O-B$ (°)	Dihedral angle between [BO ₃] triangle (°)	Average length of B-O bonds (Å)	Average length of Sr-O bonds (Å)	Angle of $\angle B-O-B$ (°)	Dihedral angle between [BO ₃] triangle (°)
13	1.3656	2.5060	130.232	18.260	1.3677	2.6145	132.546	17.706
20	1.3655	2.5060	130.232	18.260	1.3677	2.6145	132.548	17.706
40	1.3656	2.5059	130.229	18.265	1.3678	2.6148	132.549	17.725
60	1.3656	2.5060	130.225	18.277	1.3678	2.6149	132.531	17.771
80	1.3656	2.5061	130.223	18.294	1.3678	2.6151	132.531	17.785
100	1.3656	2.5062	130.221	18.310	1.3678	2.6153	132.508	17.811
120	1.3656	2.5064	130.220	18.332	1.3678	2.6154	132.504	17.825
140	1.3656	2.5065	130.216	18.348	1.3678	2.6154	132.495	17.852
160	1.3656	2.5069	130.222	18.368	1.3678	2.6155	132.490	17.857
180	1.3657	2.5074	130.225	18.399	1.3678	2.6156	132.482	17.882
200	1.3657	2.5077	130.222	18.424	1.3678	2.6160	132.482	17.898
220	1.3657	2.5079	130.219	18.453	1.3678	2.6164	132.484	17.924
240	1.3657	2.5083	130.217	18.458	1.3678	2.6167	132.481	17.950
260	1.3657	2.5085	130.215	18.506	1.3679	2.6171	132.480	17.973
280	1.3658	2.5089	130.215	18.533	1.3679	2.6174	132.475	18.003

Fig. S4 Comparison between the AE -O and B-O bond lengths in (a) CaB_2O_4 and (b) SrB_2O_4 .

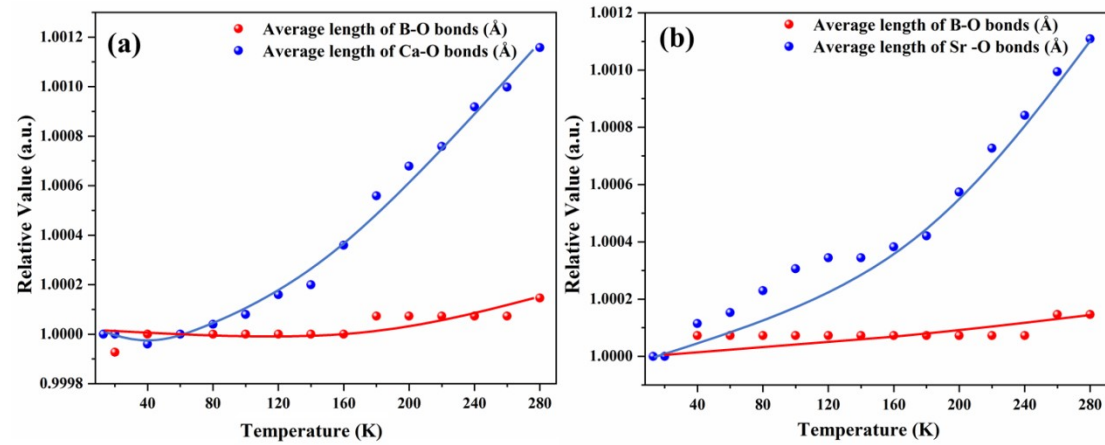


Fig. S5 Raman spectra of CaB₂O₄ from 93K to 500K.

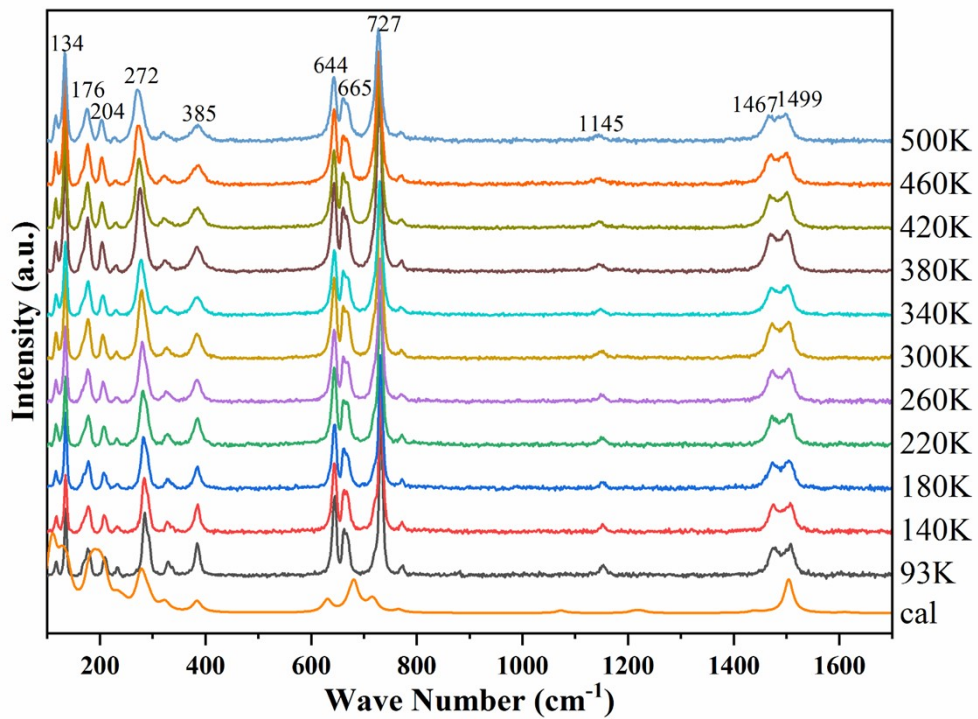


Table S5 Vibrational mode frequencies of Raman spectrum in CaB₂O₄ and SrB₂O₄ from 93K to 500K. The values of the anomalous phonon modes are highlighted by blue color.

CaB ₂ O ₄											
Temperature (K)	mode i	mode ii	mode iii	mode iv	mode v	mode vi	mode vii	mode viii	mode ix	mode x	mode xi
93	134.3145	175.0434	209.6917	287.0761	384.3341	644.5945	666.0707	733.2475	1153.7310	1476.7820	1507.9600
140	134.0325	175.2574	208.8712	285.7429	384.6489	644.4494	665.6955	732.0308	1152.3751	1475.1241	1506.0027
180	134.0610	175.3013	208.1999	284.459	384.7014	644.3507	666.0909	731.7353	1152.0732	1474.8023	1505.9689
220	133.9208	174.9857	208.1653	284.2121	384.7009	644.4845	664.1429	731.247	1151.0834	1473.8922	1505.4281
260	134.0610	175.043	207.2933	283.4221	384.6243	643.9508	665.9178	730.8912	1050.1925	1472.5342	1503.8672
300	134.0521	174.943	206.2138	281.595	385.1243	644.3342	666.2987	729.8349	1049.2734	1471.9998	1503.9138
340	133.4303	174.8287	205.7569	279.7791	384.0718	643.7301	666.2987	730.1385	1048.7733	1470.0163	1502.4894
380	133.3135	174.6332	204.8849	277.9412	383.8095	643.6832	666.0709	728.7289	1147.2233	1470.3193	1501.9864
420	132.7997	174.4805	204.6205	277.3982	385.2261	643.2593	665.7749	728.0312	1146.5678	1469.9070	1500.3584
460	132.8230	174.2556	204.4281	276.6081	385.4321	643.6295	665.4593	727.9024	1145.6546	1469.0001	1499.5561
500	132.7800	174.1972	202.2274	273.2441	385.7051	642.8743	665.9424	727.5217	1144.7765	1468.5108	1499.6681
Tendency	constant to soften	constant to soften	soften	soften	harden	constant	constant	soften	soften	soften	soften
SrB ₂ O ₄											
Temperature (K)	mode i	mode ii	mode iii	mode iv	mode v	mode vi	mode vii	mode viii	mode ix	mode x	mode xi
93	143.2768	163.0973	202.7961	254.3740	387.6074	638.1517	674.6501	724.5840	1143.638	1461.8886	1492.2874
140	143.3991	163.2048	202.9250	253.2314	388.3388	638.1033	675.0308	724.0666	1142.8017	1461.3743	1491.8595
180	143.7255	163.0973	202.9251	252.1958	388.1094	638.1517	675.5846	723.8314	1141.4788	1458.7196	1490.068
220	143.6031	163.8926	202.2372	251.3388	388.8434	638.2513	675.7576	723.339	1141.1276	1460.5184	1490.4884
260	143.2587	164.9243	202.2372	250.6646	389.4397	638.3685	675.9307	723.3140	1139.8219	1460.9468	1490.4884
300	143.5011	165.5046	201.6569	249.8212	389.6920	638.5448	675.5846	722.6084	1138.4618	1460.0045	1489.1188
340	142.4470	165.1627	200.3461	247.8542	389.5970	638.4243	676.2124	722.0865	1136.6697	1459.892	1488.8568
380	141.9843	164.5307	199.8194	246.8008	390.2749	638.3849	675.9080	721.7690	1135.8418	1459.6323	1488.8568
420	141.5215	164.3718	199.6472	246.1688	391.3622	638.4476	675.6037	721.4022	1135.6747	1459.3452	1487.8577

460	140.9661	164.1777	199.4194	243.9566	392.1389	638.3181	675.9689	721.2690	1135.6045	1459.0451	1486.8575
500	140.8661	164.0041	199.1874	242.7979	392.4495	638.2994	676.2733	719.1586	1134.2753	1457.0331	1485.2082
Tendency	constant to soften	harden to soften	soften	soften	harden	constant	harden	soften	soften	soften	soften

Fig. S6 Raman peaks shifting tendency *versus* temperature of (a) CaB₂O₄ and (b) SrB₂O₄.

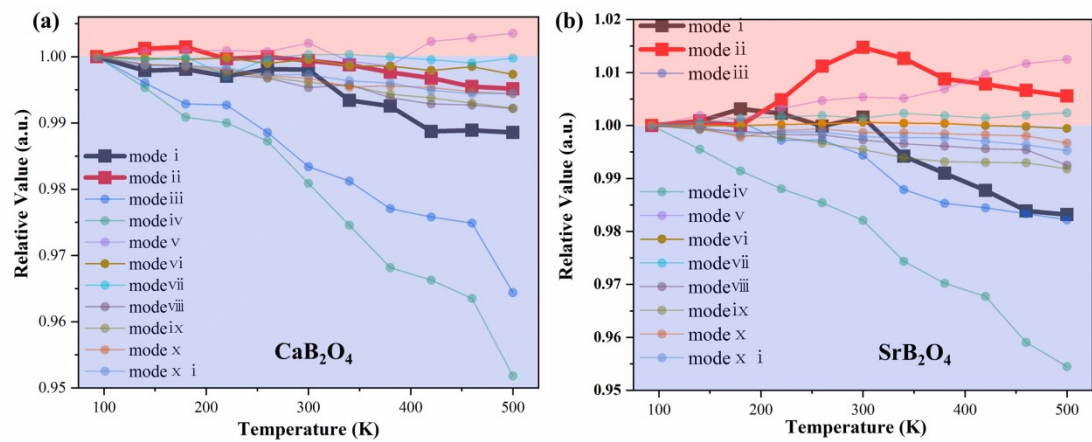
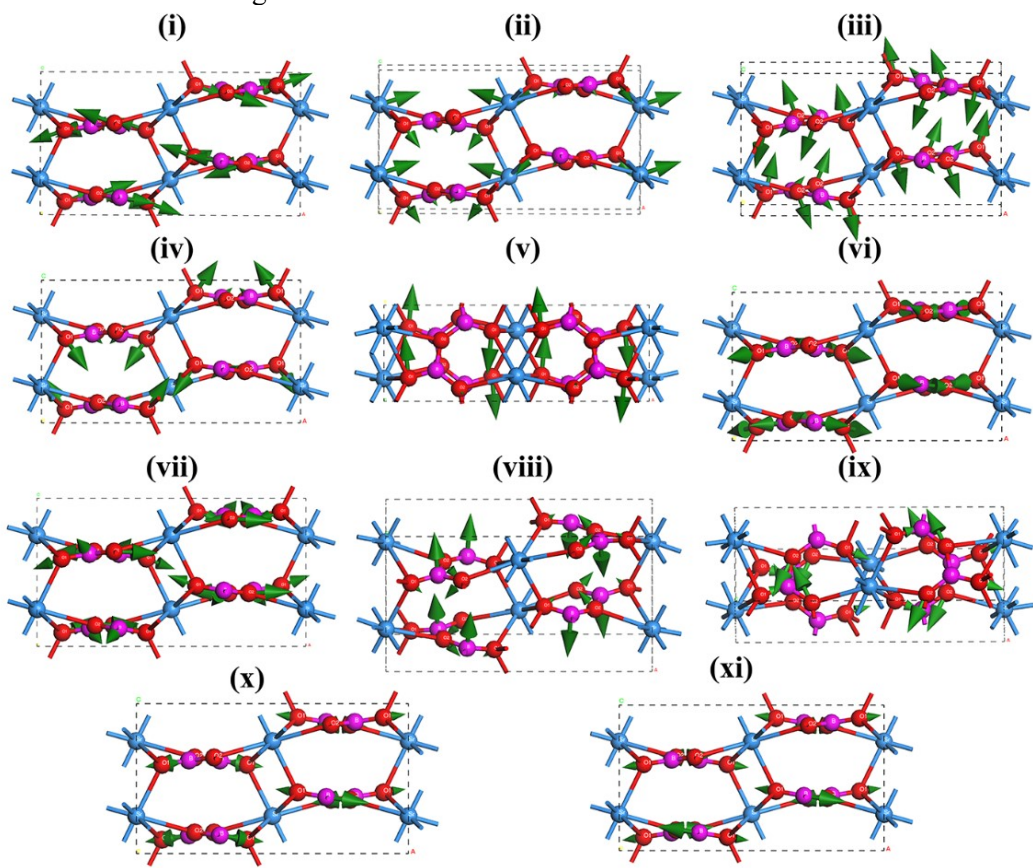


Fig. S7 Atomic vibration assignment for modes i to xi .



Reference

1. B. AXS, *Bruker AXS TOPAS V4: General profile and structure analysis software for powder diffraction data. – User's Manual*, Karlsruhe, 2008.
2. M. J. Cliffe and A. L. Goodwin, *J. Appl. Cryst.*, 2012, **45**, 1321-1329.
3. D. A. Dows and V. Schettino, *J. Chem. Phys.*, 1973, **58**, 5009-5016.
4. S. J. Clark, M. D. Segall, C. J. Pickard, P. J. Hasnip, M. J. Probert, K. Refson and M. C. Payne, *Z. Kristallogr.*, 2005, **220**, 567-570.
5. W. Kohn and L. J. Sham, *Phys. Rev.*, 1965, **140**, 1133.
6. J. P. Perdew, K. Burke and M. Ernzerhof, *Phys. Rev. Lett.*, 1996, **77**, 3865-3868.
7. J. P. Perdew and Y. Wang, *Phys. Rev. B*, 1992, **46**, 12947-12954.
8. D. R. Hamann, M. Schluter and C. Chiang, *Phys. Rev. Lett.*, 1979, **43**, 1494-1497.
9. L. Kleinman and D. M. Bylander, *Phys. Rev. Lett.*, 1982, **48**, 1425-1428.
10. H. J. Monkhorst and J. D. Pack, *Phys. Rev. B*, 1976, **13**, 5188-5192.
11. B. G. Pfrommer, M. Cote, S. G. Louie and M. L. Cohen, *J. Computat. Phys.*, 1997, **131**, 233-240.
12. S. Baroni, S. de Gironcoli, A. Dal Corso and P. Giannozzi, *Rev. Mod. Phys.*, 2001, **73**, 515-562.
13. C. Adamo and V. Barone, *The J. Chem. Phys.*, 1999, **110**, 6158-6170.
14. Z. Lin, X. Jiang, L. Kang, P. Gong, S. Luo and M.-H. Lee, *J. Phys. D:Appl. Phys.*, 2014, **47**.
15. P. E. D, *Handbook of Optical Constants of Solids*, Academic, New York, 1985.
16. Physics A(1972). American Instituteof Physics Handbook(McGraw-Hill Book Company)..
17. E. R. Dobrovinskaya, L. A. Lytvynov and V. Pishchik, in *Sapphire*, 2009, pp. 55-176.
18. J. Fontanella, R. L. Johnston, J. H. Colwell and C. Andeen, *Applied Optics*, 1977, **16**, 2949-2951.
19. C. Moelle, S. Klose, F. Szucs, H. J. Fecht, C. Johnston, P. R. Chalker and M. Werner, *Diamond and Related Materials*, 1997, **6**, 839-842.
20. I. H. Malitson, *Journal of the Optical Society of America*, 1962, **52**, 1377-1379.
21. D. N. Batchelder and R. O. Simmons, *J. Chem. Phys.*, 1964, **41**, 2324-2329.